Available online at www.sciencedirect.com
SCIENCE DIRECT®
Journal of Chromatography A, 1073 (2005) 111–121
JOURNAL OF CHROMATOGRAPHY A
www.elsevier.com/locate/chroma

Investigation of the steric mass action formalism in the simulation of breakthrough curves on a monolithic and a packed bed column

Magdalena Jozwik [a], Krzystof Kaczmarski [b], Ruth Freitag [a, c, *]

[a] *Laboratory of Chemical Biotechnology, Swiss Federal Institute of Technology Lausanne, Switzerland*
[b] *Faculty of Chemistry, Rzeszow University of Technology, Rzeszow, Poland*
[c] *Chair for Process Biotechnology, University of Bayreuth, D-95440 Bayreuth, Germany*

Available online 16 February 2005

Abstract

The simulation of the behaviour of two proteins (cytochrom *c* and α-chymotrypsinogen) on two types of stationary phases (monolithic and porous particle-based) was attempted for non-linear (simulation of breakthrough curves) and linear (simulation of elution peaks) cation exchange chromatography. It was found that the combination of a stoichiometric model (steric mass action, SMA) with the lumped pore diffusion (POR) model allows a simulation of high predictive value. Using one set of SMA and transport parameters for a given column morphology and/or protein, breakthrough curves and peaks could be simulated that agreed well with the experimental data while no dependency on either the protein load or the mobile phase composition (salt content) was observed. One of the SMA parameters, namely the characteristic charge needed some slight adjustment (within the error of the experimental determination of this parameter) in order to optimise the fit.

Keywords: SMA; Proteins; POR

1. Introduction

Model-based approaches increasingly contribute to efficient bioprocess development and performance. One area that is known to create a major part of the costs in the production of high value bioproducts such as proteins and which could therefore profit significantly from predictive modelling, is the downstream process and here especially preparative chromatography. Numerous kinetic models are available to account for the band profile development in chromatography [1–6]. Combined with isotherm data these should in principle allow the simulation and concomitantly the in silico development and optimisation of the separation.

In non-linear chromatography peak shape and spreading are complex functions of the equilibrium isotherms, the mass transfer parameters (film mass transfer coefficients and intraparticle diffusivity), as well as certain design (particle size and column length) and operating parameters (pulse size, feed concentration and flow rate) [7–12]. For the purpose of modelling, the process is usually divided into three discrete steps, namely mass transfer from bulk liquid to the outer surface of the stationary phase particles (film-diffusion resistance/external mass transfer resistance), movement by diffusion into the pores of the adsorbent (pore diffusion, internal mass transfer resistance), and binding to the adsorptive surface (surface-reaction resistance).

The kinetic models differ in their degree of flexibility in taking these effects into account. The general rate model is by far the most comprehensive one [3,4,13]. In this model, axial dispersion and the mass transfer resistances are calculated individually. In many ways it is a very attractive model, as it allows the development of equations based on assumptions concerning the actual physical behaviour of the proteins under chromatographic conditions. The GR model does however, require knowledge of a large number of experimental values that are difficult to determine and hence the model is awkward to use.

When the mass transfer resistances are small and have a minor influence on the profiles, models like the equilibrium-dispersive (ED) or the transport-dispersive (TD) model can be used [4,14–16]. Such models lump several effects together.

* Corresponding author. Tel.: +49 921 55 7371; fax: +49 921 55 7375.
E-mail address: ruth.freitag@uni-bayreuth.de (R. Freitag).

0021-9673/$ – see front matter © 2005 Elsevier B.V. All rights reserved.
doi:10.1016/j.chroma.2005.01.059

They are easy to apply, require only a few simply determined experimental parameters and as a consequence enjoy much popularity. However, the predictive value of such models is limited, since the involved lumped mass transfer and dispersion parameters are physically meaningless. In some cases these parameters have, e.g., shown an inexplicable dependency on the sample concentration [17].

The lumped pore diffusion (POR) model used in this paper lays in complexity between the GR and the ED/TD models and is in fact a simplification of the GR model [14,17–19]. The POR model needs the same set of parameters as the GR model, but can be solved much faster. As Kaczmarski and co-workers [17,20] were recently able to demonstrate, the POR model can replace the GR model without loss in predictive power, in particular when

$$Pe > 100 \quad \text{and} \quad \frac{St}{Bi} > 5,$$

where Pe is the Peclet number ($uL/(DL\varepsilon_e)$), St the Stanton number ($St = k_{ext}a_pL\varepsilon_e/u$), Bi the Biot number ($Bi = k_{ext}d_p/2D_{eff}$), u the mobile phase velocity, d_p the average particle diameter, L the column length, a_p the external surface area of the adsorbent particles, ε_e the external porosity, k_{ext} the external mass transfer coefficient, and D_{eff} is the effective diffusion coefficient.

In order to model experimental band profiles the kinetic models need to be linked with an adsorption isotherm formalism. Since experimental protein isotherms on various stationary phase materials can usually be fitted well to the Langmuir equation or one of its various modified forms [21–23], these Langmuir algorithms are generally used to model the breakthrough curves in protein chromatography. However, the use of the Langmuir formalism has some drawbacks. Unless the saturation capacities of all involved proteins are identical, the approach is thermodynamically inconsistent. Moreover, the steric hindrance effects exerted by the adsorbed protein molecules or surface interactions between them cannot be taken properly into account. Several more suitable approaches to protein isotherm formulation can be found in the literature, see below. However, the majority of these isotherms have to date only been used in combination with the more simple ED/TD kinetic models.

The ion-exchange process is largely governed by electrostatic interactions. However, the exact mechanism by which adsorption occurs is still unknown. Boardman and Partridge [24] have given a theoretical treatment for ion exchange of polyelectrolytes on weak cation exchangers. This approach was based on a stoichiometric exchange between the protein and the counter ions to the fixed charges on the stationary phase surface. Synergistic effects were not taken into consideration. This theory has since then been used in several alternative formulations such as the multivalent ion exchange formalism or the stoichiometric displacement model [25,26]. Experimentally observed characteristics of proteins adsorption such as irreversible binding, sensitive dependence of protein retention on the salt concentration, and the depression of single component isotherms in the presence of competing solutes are well described by this approach.

The major fallacy of the stoichiometric adsorption models, is that in these models the binding of a solute to the stationary phase is assumed to affect only a number of ion exchange groups on the stationary phase surface equal to the characteristic charge of the adsorbed molecule. However, as suggested by Velayudhan and Horvath [27], bound macromolecules, by virtue of their size, cover significantly more sites (and bound counter ions) than that. In fact, this steric shielding of ion exchange groups/counter ions plays a major role in the behaviour of protein in ion exchange chromatography. Cramer and co-workers [28,29] have developed a stoichiometric approach in the form of the steric mass action (SMA) model, in which the possible effect of sterically hindered exchange sites is included. The SMA formalism is specifically designed for representing multicomponent protein–salt equilibria in ion exchange chromatography based on the following assumptions:

- The solution and adsorbed phases are thermodynamically ideal allowing the use of concentrations instead of activities.
- The multipoint nature of protein binding can be represent by an experimentally determined characteristic charge.
- Competitive binding can be represented by the law of mass action where the electroneutrality on the stationary phase is maintained.
- The binding of large molecules causes a steric hindrance of salt counter ions bound to the adsorptive phase, which become unavailable for exchange with other solutes.
- The effect of the co-ion can be neglected in the ion-exchange process.

Assuming that electrostatic interaction is the only mechanism involved during adsorption, the stoichiometric exchange of a polyelectrolyte (protein) and the small counter ions can be represent by Eq. (1).

$$C_P + \nu_P\bar{Q}_S \Leftrightarrow Q_P + \nu_P C_S \tag{1}$$

where C and Q are the mobile and stationary phase concentrations, ν the characteristic charge and subscripts P and S refer to the protein and salt respectively. The overbar denotes salt ions available for free exchange with other solutes.

The equilibrium constant is defined as

$$K_P = \left(\frac{Q_P}{C_P}\right) \times \left(\frac{C_S}{\bar{Q}_S}\right)^{\nu_D} \tag{2}$$

Electroneutrality on the stationary phase requires that

$$\Lambda \equiv \bar{Q}_S + (\nu_P + \sigma_P) \times Q_P \tag{3}$$

where Λ [mM] is the ion capacity of the column and σ is the steric factor of the protein.

The following implicit isotherm can then be written for the protein by combining Eqs. (2) and (3).

$$C_P = \left(\frac{Q_P}{K_P}\right)\left(\frac{C_S}{\Lambda - (\nu_P - \sigma_P)Q_P}\right)^{\nu_P} \quad (4)$$

Once Q_P is known $\bar{Q}_S$ may be calculated from Eq. (3), while the total concentration of salt counter ions Q_S is given by $Q_S = \bar{Q}_S + (\sigma_P Q_P)$.

Physically, the characteristic charge represents the number of ion exchange groups on the stationary phase surface involved in the ion exchange reaction with the protein, the steric factor represents the number of counter-ions on the adsorbent surface, which are unavailable for exchange with other molecules in solution due to the shielding by the adsorbed protein, while the equilibrium constant is a measure of the affinity of the macromolecule to the stationary phase [30].

While the SMA model takes shielding and steric hindrance effects well into account, equilibrium parameters in the SMA formalism are taken as constant and independent of the solute and counter ion concentration. Non-ideal effects such as aggregation or changes in the tertiary structure of the protein, but also other potential deviation from the ideal stoichiometric case such as van der Waals and electrostatic interactions between adsorbed proteins and the salt ions, or secondary (e.g. hydrophobic) interactions between the proteins and the adsorbate escape consideration. In most cases these can be ignored. If not, the combination of the SMA approach with the non-ideal surface solution model (NISS) proposed by Li and Pinto [31] may be used.

The results reported in this paper are part of a general effort towards modelling highly non-linear chromatographic separations such as protein displacement chromatography [32–35]. We have recently shown that the Langmuir formalism is not suited for this purpose in our case [36]. In this paper we intend to show that a stoichiometric adsorption equilibrium model, namely the SMA algorithm, may be more useful. Ion exchange chromatography was chosen as example, since it is a popular method in preparative protein chromatography allowing efficient protein separation while maintaining the native structure and hence the biological activity of the product to the highest degree.

2. Materials and methods

2.1. Materials

α-Chymotrypsinogen A from bovine pancreas and cytochrom *c* from bovine heart as well as sodium phosphate and sodium chloride for buffer and eluent preparation were from Sigma (St Louis, MO, USA). The purity of the proteins was determined by matrix assisted laser-induced desorption ionisation time-of-flight mass spectrometry (MALDI-TOF MS, Atheris, Geneva, Switzerland). Water was purified using an Elix-3 system (Millipore, Bedford, MA, USA). Columns and stationary phases were from Bio-Rad (Herkules, CA, USA). The porous particle-based column was a BioScale S2 filled with 10 μm Macro-Prep S particles (nominal average pore size 1000 Å). The beads consist of a highly hydrophilic methacrylate-based support, to which strong cation exchanger groups ($-SO_3^-$) are linked. The monolithic column was a UNO S1. The exact composition of the UNO column is proprietary, but the material is also highly hydrophilic and $-SO_3^-$ groups provide again the cation exchange capability.

2.2. Instrumentation

The experiments were carried out using a system assembled from a model 422 HPLC pump (Bio-Tek Kontron Instruments, Basel, Switzerland), a Valco 10-port valve (Valco, Houston, TX, USA), and a HPLC UV detector (Bio-Tek Kontron Instruments, Basel, Switzerland). Data collection and processing was by PC.

2.3. Chromatography

All isotherm measurements by frontal chromatography [37,38] were carried out at ambient temperature in the indicated mobile phase. The solvents used to prepare the mobile phase were filtered before use on SFCA filter membrane 0.2 (m pore size (Suwannee, GA, USA). For an isotherm measurement the column was equilibrated with the mobile phase. Then the flow was switched to a solution containing the protein of interest at a given concentration in the mobile phase and the breakthrough curve was recorded. Mass conservation of the solute between the time when the new solution enters the column and a final time for which the plateau concentration is reached, allows the calculation of the adsorbed amount of the solute in the stationary phase at equilibrium with a given concentration in the mobile phase. The adsorbed amount Q_P^* is given by:

$$Q_P^* = \frac{C_P(V_{eq} - V_0)}{V_a} \quad (5)$$

where V_{eq} and V_0 are the elution volume of the equivalent area and the hold-up volume, and V_a is the volume of the stationary phase.

For column regeneration between each frontal analysis measurement the column was flushed with 2 M NaCl. Break through curves and elution peaks were recorded at a flow rate of 0.5 mL/min.

2.4. Computational methods

The programs used to perform the numerical calculations discussed in this work were written using the method of orthogonal collocation on finite elements [4,15,39,40].

2.5. Kinetic models

In the POR model the mass balances of the *i*th component in the mobile and solid phase are the following:

$$\varepsilon_e \frac{\partial C_{P,i}}{\partial t} + u\frac{\partial C_{P,i}}{\partial z} = \varepsilon_e D_L \frac{\partial^2 C_{P,i}}{\partial z^2} - (1-\varepsilon_e)k_i a_p (C_{P,i} - \bar{C}_{P,i}) \quad (6a)$$

$$\varepsilon_p \frac{\partial \bar{C}_{P,i}}{\partial t} + (1-\varepsilon_p)\frac{\partial \bar{Q}_{P,i}}{\partial t} = k_i a_p (C_{P,i} - \bar{C}_{P,i}) \quad (6b)$$

where $\bar{C}_P$ and $\bar{Q}_i$ denote average concentrations in the stagnant fluid phase contained in the pore of the stationary phase and k_i is the overall mass transfer coefficient of component *i*.

In solving these partial differential equations, the following initial conditions were used:

$$C_{P,i}(0,z) = C_i^0, \quad \bar{C}_{P,i}(0,z) = 0, \quad \text{and} \quad \bar{Q}_{P,i}(0,z) = 0 \quad \text{for } 0 < z < L. \quad (7)$$

In addition, two sets of boundary conditions apply, one at the column inlet, the other at the column outlet. For $t > 0$ and $z = 0$ (inlet) the condition is:

$$u_f C'_{P,f,i} - u(0)C(0) = -\varepsilon_e D_L \frac{\partial C_{P,i}}{\partial z} \quad C'_{P,f,i} = C^0_{P,f,i}; \quad \text{for } 0 < t < t_P \quad C'_{P,f,i} = 0 \quad \text{for} \quad t = t_P \quad (8)$$

The condition for $t > 0$ and $z = L$ (outlet) is:

$$\frac{\partial C_{P,i}}{\partial z} = 0 \quad (9)$$

The axial dispersion coefficient, D_L, was calculated from the Gunn equation [41]:

$$\varepsilon_e \frac{D_L}{d_p u} = \frac{ReSc}{4\alpha_1^2(1-\varepsilon)}(1-p)^2 + \left(\frac{ReSc}{4\alpha_1^2(1-\varepsilon_e)}\right)^2 p(1-p)^3 \times \left(\frac{-4\alpha_1^2 11(1-\varepsilon_e)}{p(1-p)ReSc}\right)\frac{\varepsilon_e}{\gamma ReSc} \quad (10)$$

where p is equal to $0.17 + 0.33\,10^{-24/Re}$ and Sc and Re are the Schmidt and the Reynolds numbers, respectively, with $Sc = \eta/(\rho D_m)$, and $Re = (\rho u d_p)/\eta$.

The overall mass transfer coefficient k_i of component *i* is given by the following relationship:

$$k_i = \left[\frac{1}{k_{ext,i}} + \frac{1}{k_{int,i}}\right]^{-1} \quad (11)$$

where $k_{ext,i}$ and $k_{int,i}$ are the external and the internal mass transfer coefficients, respectively. The internal mass transfer coefficient can be calculated as follows:

$$k_{int,i} = \frac{10 D_{eff,i}}{d_p}, \quad \text{with} \quad D_{eff,i} = \frac{\varepsilon_p D_{m,i}}{\gamma} \quad (12)$$

where the correlation proposed by Young and Carroad [42] was used for estimating the value of the molecular diffusion coefficient, $D_{m,i}$.

$$D_{m,i} = 8.34 \times 10^{-8} \times \frac{T}{\eta \times M^{0.3}} \quad (13)$$

T is the temperature, η the viscosity of the solvent, and M the molecular weight of the compound in question.

The tortuosity factor γ was calculated according to $\gamma = (2-\varepsilon_p)^2/\varepsilon_p$, where ε_p is the particle porosity, which was calculated according to Eq. (14),

$$\varepsilon_t = \varepsilon_e + (1-\varepsilon_e)\varepsilon_p \quad (14)$$

where ε_t is the total column porosity measured using acetone as inert tracer and ε_e is the external column porosity obtained from the sodium nitrate elution peak.

The value of the external mass transfer coefficient was calculated from the Sherwood number, *Sh*, according to the Wilson–Greankoplis correlation [43]

$$Sh = \frac{k_{ext,i} d_p}{D_m} = \frac{1.09}{\varepsilon_e} Sc^{1/3} Re^{1/3} \quad (15)$$

In case of the monolithic column an apparent average particle diameter was estimated by measuring the pressure drop over the column as a function of the flow rate and applying the Carman–Kozeny equation [44].

2.6. SMA model parameters

The ion capacity of the stationary phase, Λ, was determined as follows; the column was first equilibrated with a 120 mM sodium phosphate buffer pH 7.2 for approximately 10 column volumes followed by a front of a solution containing 1 M ammonium sulphate in water. The bed capacity was then determined by measuring the amount of sodium ions displaced by the ammonium ions using atomic absorption spectrometry. Fractions were diluted 100 times in UHP water prior to measurements. Na^+ ion standards in the range of 10–200 mg/L were used for the calibration.

The characteristic charge, ν, the steric factor, σ, and the adsorption equilibrium constant, K, for the proteins were obtained according to the protocol described by Brooks and Cramer [28]. In particular, linear elution experiments were carried out at various mobile phase salt concentrations in order to determinate ν and K according to the following equation:

$$\log k' = \log(\beta K_P \Lambda^{\nu_P}) - \nu_P \log C_s \quad (16)$$

where k' is the capacity factor, β is the column phase ratio and C_s is the initial salt concentration in the carrier. The phase ration, β was calculated according to

$$\beta = \frac{1-\varepsilon_t}{\varepsilon_t} \quad (17)$$

where $\varepsilon_t = 0.84$ and $\varepsilon_t = 0.7$ are the total porosity of the BioScale and UNO columns, respectively.

The steric factor for the proteins was obtained from frontal chromatographic experiments according to expression 18:

$$\sigma_p = \frac{\beta}{C_{P,f}\Pi}\left[\Lambda - C_S\left(\frac{\Pi}{\beta K_p}\right)^{1/\nu_p}\right] - \nu_p \quad (18)$$

where

$$\Pi = \left(\frac{V_p}{V_0} - 1\right)$$

All experiments for the determination of the SMA parameters were repeated at least three times.

3. Results and discussion

3.1. Isotherm measurements

Two simple proteins were chosen as example in this investigation of the adsorption behaviour of proteins to a strong cation exchanger column, namely cytochrom *c* from

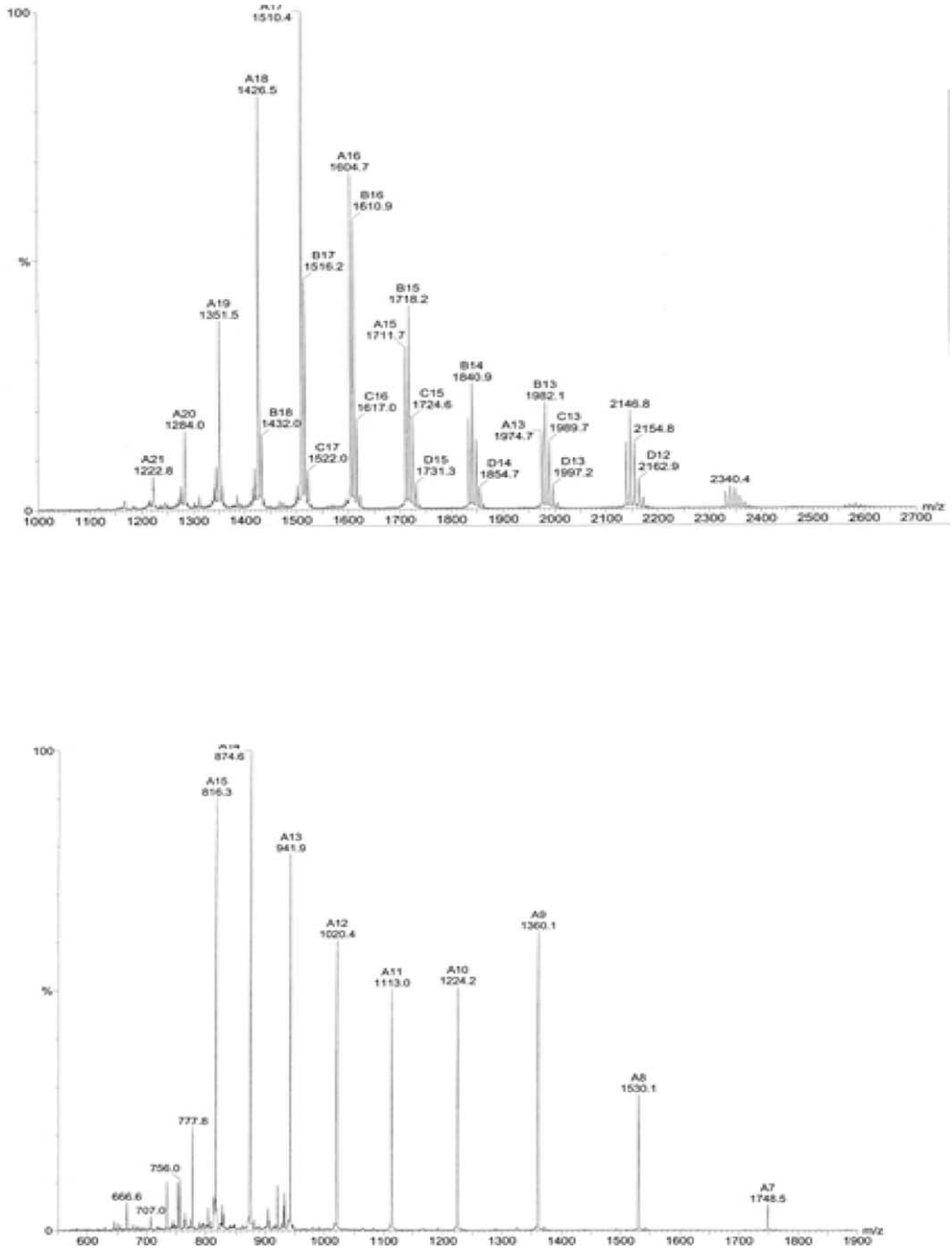

Fig. 1. MALDI (matrix assisted laser desorption ionisation) mass spectra of top: cytochrom *c* and bottom: α-chymotrypsinogen.

Table 1
Characteristic parameters of the BioScale S2 and UNO S1 columns

Parameter	BioScale S2	UNO S1
Column dimensions[a]	5.2 cm × 0.7 cm	3.5 × 0.7 cm
Column volume[a]	2 mL	1.3 mL
Column dead volume	1.7 mL	0.9 mL
Stationary phase volume	0.3 mL	0.4 mL
Total porosity, ε_t	0.85	0.70
External porosity, ε_e	0.37	0.55
Particle porosity, ε_p	0.76	0.33
Interactive group[a]	$-SO_3^-$	$-SO_3^-$
Particle/pore size[a]	10 ± 3 μm	monolith
Ion capacity (Na^+)	1833 mM	445 mM
Protein capacity (cytochrom *c*)	30 mg/mL	7 mg/mL [75 mM] 1.4 mg/mL [120 mM]
Protein capacity (α-chymotrypsinogen)	4.5 mg/mL	0.6 mg/mL
Phase ratio β	0.1	0.4
Plate number (per column)[b]	1000 ± 15%	1200 ± 15%

[a] Information supplied by the manufacturer, Bio-Rad.
[b] Determined with acetone (2%, v/v) as inert tracer at a flow rate of 0.5 mL/min.

bovine heart (mass 11572, isoelectric point 9.5) and α-chymotrypsinogen A from bovine pancreas (mass 25600, isoelectric point 8.5). The MALDI mass spectra of the two proteins, Fig. 1, showed that the cytochrom *c* was very pure, while the α-chymotrypsinogen contained some impurities. Two column morphologies were investigated, a conventional porous particle based one (BioScale S2) and a 'monolithic' one, namely the UNO S1. The characteristic parameters of the two columns are compiled in Table 1. With 1.3 mL compared to 2.0 mL, the total volume of the UNO column is about 30% less than that of the BioScale one. With 0.4 mL for the UNO and 0.3 mL for the BioScale column, the difference in the stationary phase volume is less pronounced and even slightly in favour of the monolith.

Isotherms were recorded for the two proteins on the two column types, Fig. 2. The buffer concentrations used in these experiments, i.e. a concentration of 120 mM in case of the BioScale column and of 75 mM in the case of the UNO column had been optimised during previous experiments [36]. Most of the recorded experimental isotherms show points of inflections and in some cases several steps/plateaux can be distinguished. This is the case not only for the α-chymotrypsinogen, where some impurities were present, but also for the pure cytochrom *c*. The protein capacity of the porous particle-based BioScale column is nearly four times higher than that of the monolithic UNO column, in spite of the slightly lower stationary phase volume measured for the BioScale column. The same is incidentally true for the Na^+-ion capacity, Table 1. More importantly, pronounced differences can be observed for a given column between the saturation capacities of the two proteins. For both column morphologies, the cytochrom *c* capacity is roughly ten times as high as that determined for α-chymotrypsinogen. Such differences in the saturation capacities will render the Langmuir approach unsuitable in the simulation of separations of the

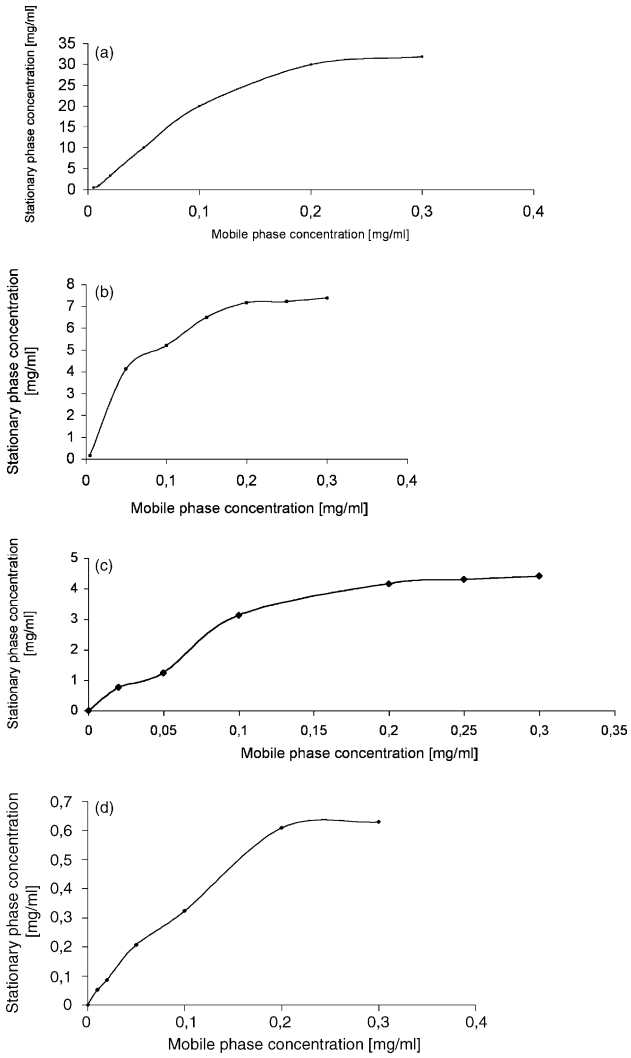

Fig. 2. Single component adsorption isotherms measured for (a) bioscale column, cytochrom *c*, (b) UNO column, cytochrom *c*, (c) bioscale column, α-chymotrypsinogen, (d) UNO column, α-chymotrypsinogen. Conditions: mobile phase, 120 mM phosphate pH 7.2 (BioScale column)/75 mM phosphate pH 7.2 (UNO column); flow rate, 0.5 mL/min.

involved proteins. As expected, isotherms were suppressed in the presence of salt, i.e. when a certain amount of NaCl was added to the mobile phase, see Fig. 3 for an example.

3.2. Determination of the SMA parameters

Subsequently the SMA parameters of the two proteins were determined for the two column morphologies according to the standard procedures outlined in the materials and methods section, Table 2. The values measured for both columns are comparable to those found in the pertinent literature for these or similar proteins [35,45,46]. The characteristic charge of both proteins is higher when measured for the in porous particle-based column than in case of the monolithic one. It was verified that these differences are not due to the difference in the mobile phase composition, namely 120 mM

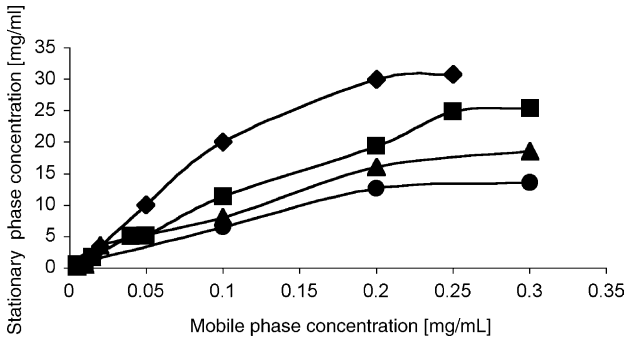

Fig. 3. Single component adsorption isotherms of cytochrom *c* measured for the BioScale S2 column in the presence of increasing amounts of salt (NaCl) in the mobile phase (120 mM phosphate, pH 7.2), (♦) 0% NaCl, (■)1% NaCl, (▲) 3% NaCl, (●)5% NaCl, flow rate: 0.5 mL/min.

Table 2
SMA parameters used in the simulations

	Cytochrom *c*	α-Chymotrypsinogen
Characteristic charge (BioScale/UNO)	2.14/0.75	0.46/0.39
Steric factor (BioScale/UNO)	49/4.9 × 10^3	8.5 × 10^3/1.5 × 10^3
Equilibrium constant (BioScale/UNO)	0.12/25.5	7.58/3.17

The experimental error in the determination of the characteristic charge is ±1.

phosphate in case of the BioScale column versus only 75 mM phosphate in the case of the UNO column. In fact, for both proteins the characteristic charge remained almost the same when the monolithic column was used with a mobile phase containing 120 instead of 75 mM phosphate buffer (e.g. 0.7 instead of 0.75 in the case of cytochrom *c*).

No clear trend can, on the other hand, be observed for the steric factor and the equilibrium constant. For α-chymotrypsinogen the values for these parameters are higher in the BioScale column, while the opposite is the case for cytochrom *c*, where both values are considerable higher in the UNO column.

3.3. Simulation of breakthrough curves

In the numerical calculation of breakthrough curves based on the POR model, the axial dispersion, D_L, as well as the external and internal mass transfer coefficients, $k_{ext,i}$ and $k_{int,i}$, are required. These were determined as described in the materials and methods section and the corresponding values are listed in Table 3 together with the molecular and effective diffusion coefficients used to calculate the mass transfer coefficients. The values for the column porosities are found in Table 1. Efficiencies (plate numbers) were determined using acetone (2%, v/v) as inert tracer at the flow rate used in the chromatographic experiments, namely 0.5 mL/min. With val-

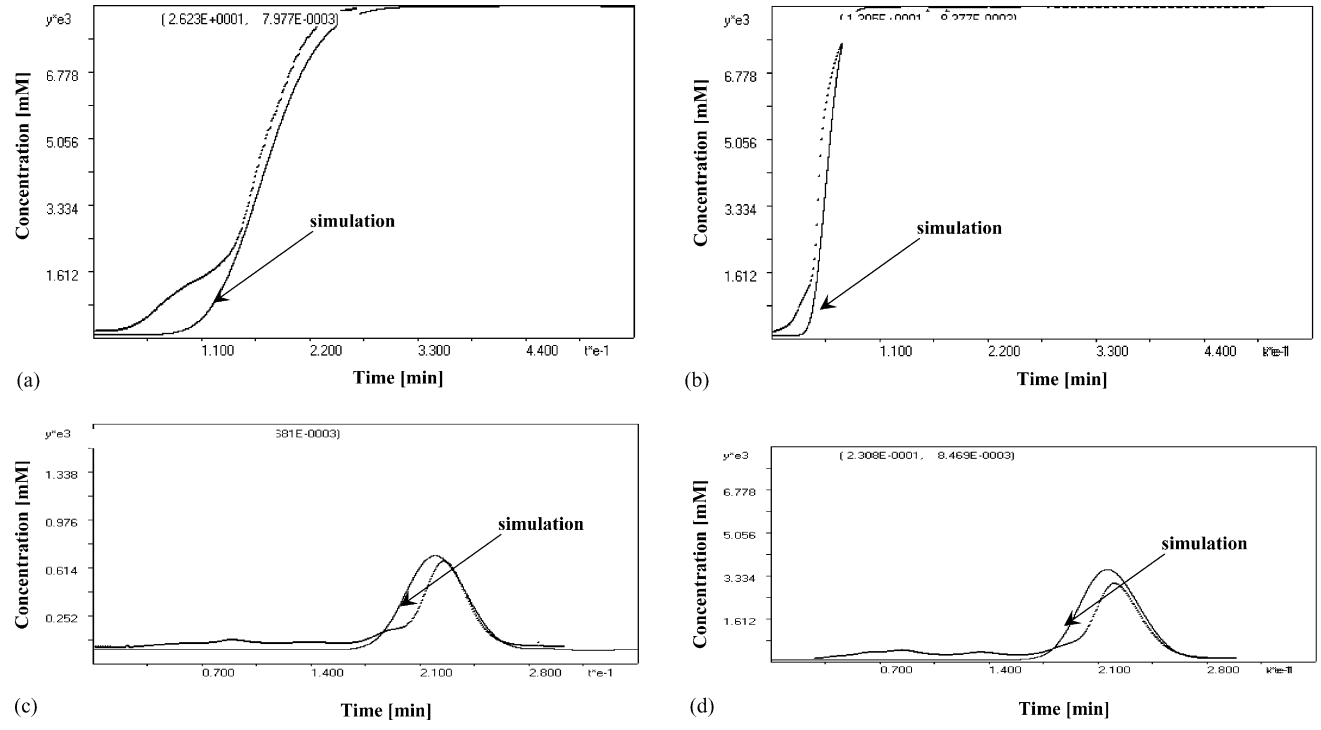

Fig. 4. Comparison between the experimental breakthrough curves and chromatograms of cytochrom *c* and the corresponding numerical solutions (solid line) as a function of the protein concentration and the mobile phase composition. Column: BioScale S2, flow rate 0.5 mL/min (a) concentration of the protein 0.0085 mM (0.1 mg/mL), mobile phase 120 mM phosphate buffer pH 7.2 + 1% NaCl (characteristic charge: 2.35), (b) concentration of the protein 0.0085 mM (0.1 mg/mL), mobile phase 120 mM phosphate buffer pH 7.2 + 10% NaCl (characteristic charge: 2.00), (c) concentration of the protein 0.0017 mM (0.02 mg/mL), mobile phase 120 mM phosphate buffer pH 7.2 (characteristic charge: 2.14), (d) concentration of the protein 0.017 mM (0.2 mg/mL), mobile phase 120 mM phosphate buffer pH 7.2 (characteristic charge: 2.14).

Table 3
Kinetic parameters of the proteins used in the simulations

	Cytochrom *c* BioScale/UNO	α-Chymotrypsinogen BioScale/UNO
D_m (cm^2/min)	3.05×10^{-5}	7.12×10^{-5}
$D_{m,P}$ (cm^2/min)	$1.0 \times 10^{-6}/1.0 \times 10^{-8}$	$1.0 \times 10^{-8}/4.5 \times 10^{-9}$
D_{eff} (cm^2/min)	$2.17 \times 10^{-5}/13.5 \times 10^{-6}$	$1.37 \times 10^{-8}/4.4 \times 10^{-9}$
D_L (cm^2/min)	$4.43 \times 10^{-3}/5.8 \times 10^{-4}$	$8.57 \times 10^{-3}/2.5 \times 10^{-3}$
k_{ext} (cm/min)	$3.14 \times 10^{-1}/7.0 \times 10^{-1}$	$2.3 \times 10^{-3}/8.1 \times 10^{-3}$
k_{int} (cm/min)	$4.1 \times 10^{-3}/4.4 \times 10^{-1}$	$4.4 \times 10^{-5}/2.0 \times 10^{-3}$

ues of 1000 (±15%) plates per column, see also Table 1, the column efficiencies should be high enough for an accurate analysis of the breakthrough curves.

These experimental values were used together with the SMA isotherm for a first simulation of breakthrough curves for both proteins on both column morphologies (mobile phase 120 mM phosphate pH 7.2 for the BioScale and 75 mM phosphate pH 7.2 for the UNO column). In all cases the initial agreement between experimental and simulated results was far from satisfactory. A systematic investigation of possible reasons revealed that the bulk molecular diffusion coefficients, $D_{m,i}$, calculated according to Eq. (13) cannot be used to calculate an effective internal diffusion coefficient respectively an internal mass transfer coefficient (Eq. (12)) that correctly describes the diffusion of the proteins inside the 'pores' of either column type. In order to demonstrate this, a value for the protein diffusivity inside the stationary phase, dubbed $D_{m,P}$, was calculated for each protein/column pair by fitting the corresponding simulated breakthrough curve to the experimental one, see Table 3 for the values. The physical basis for the thus derived diffusivities remains at present unclear. If one compares the 'fitted' $D_{m,P}$-values with the ones for the molecular respective effective diffusion coefficients calculated according to Eqs. (12) and (13), the $D_{m,P}$-value is about one order of magnitude smaller. Taking into consideration that a highly attractive chromatographic phase was used to interact with the proteins in these experiments, it is possible that the observed slow intraparticle diffusion, respectively the small internal mass transfer coefficient k_{int} was due to the fact that mass transfer inside the pores is dominated by surface rather than conventional pore diffusion.

Finally it is interesting to note that in case of the porous particle-based column for both proteins the values for the internal mass transfer coefficient are two orders of magnitude smaller than the ones for the external one. Apparently the internal mass transfer shows a major resistance in the case of the BioScale column, which is after all not surprising in the

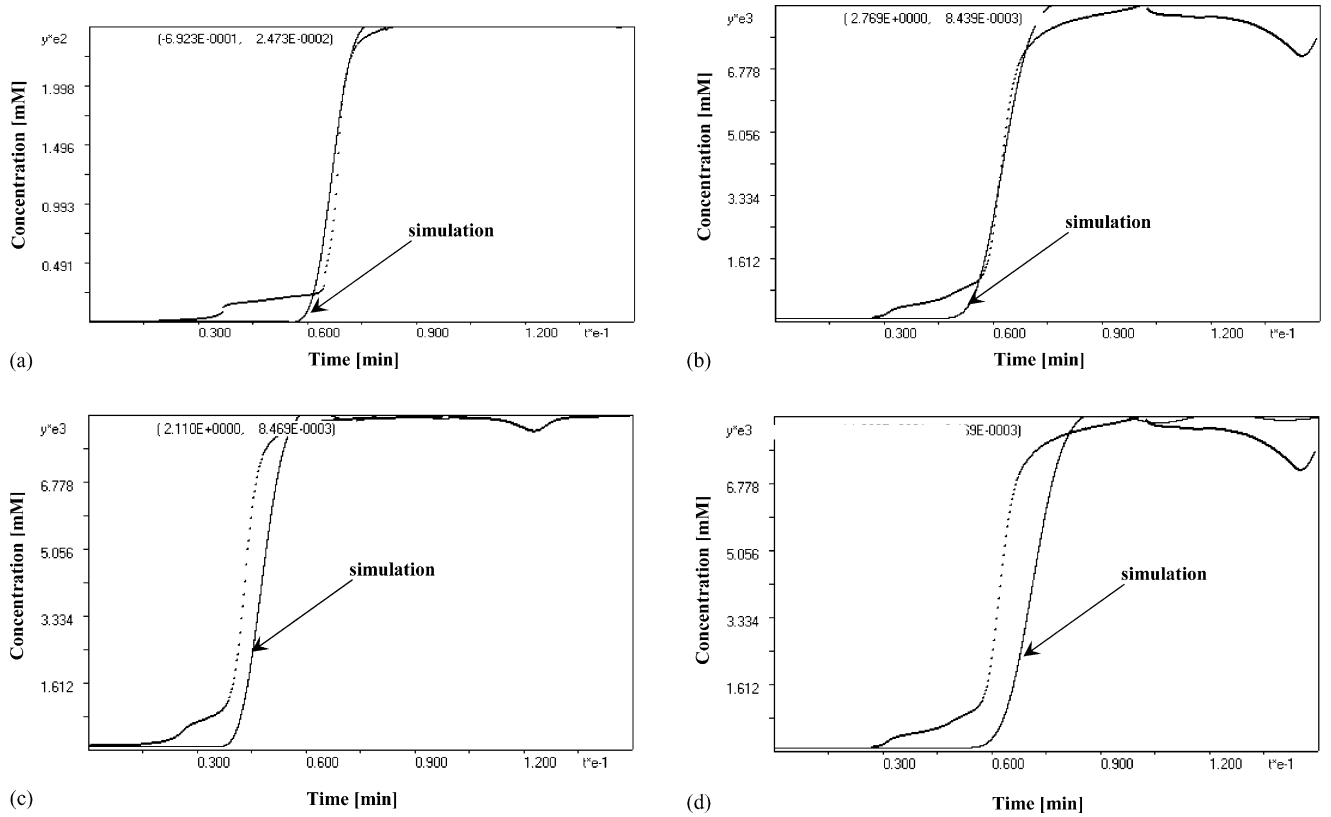

Fig. 5. Comparison between the experimental breakthrough curves and chromatograms of cytochrom *c* and the corresponding numerical solutions. Column: UNO S1, flow rate 0.5 mL/min, protein concentration: 0.025 mM (0.3 mg/mL). (a) Mobile phase: 120 mM phosphate buffer pH 7.2 (characteristic charge: 0.69), (b) mobile phase: 120 mM phosphate buffer pH 7.2 + 1% NaCl (characteristic charge: 0.49), (c) mobile phase: 120 mM phosphate buffer pH 7.2 + 3% NaCl (characteristic charge: 0.06), (d) mobile phase: 120 mM phosphate buffer pH 7.2 + 5% NaCl (characteristic charge: 0.01).

case of a porous particle-based stationary phase. In the case of the monolithic column, both mass transfer coefficients are in the same order of magnitude. It must be admitted however, that the physical meaning and the location of the internal mass transfer is somewhat unclear in the case of the monolithic column. This monolith does not have micropores filled with stagnant fluid, such structures can therefore not be held responsible for the observed behaviour. Unfortunately at present, the kinetic models of chromatography cannot take into account the specific morphology of a monolithic column. This became e.g. evident, when an (apparent) particle diameter had to be calculated in order to apply Eq. (12) for the calculation of the internal mass transfer coefficient. The equivalence of the two mass transfer coefficients could hence also mean that the differentiation between external and internal mass transfer was arbitrary in the case of the UNO column, as only one mass transfer process by diffusion—that of the bulk mobile phase to the surface of the monolith—occurred.

The fitted coefficient for internal diffusion ($D_{m,P}$-value) was subsequently used together with the corresponding SMA parameters to simulate breakthrough curves and elution peaks of cytochrom *c* on the BioScale S2 column for different protein concentrations and mobile phase compositions, using a combination of the POR model and the SMA isotherm formalism. In each case the same diffusion coefficient could be used to model the behaviour independent of the protein concentration or the mobile phase composition in the investigated range (0.02–0.2 mg/mL protein, 0–10% NaCl), Fig. 4. The calculated breakthrough curves and peaks were found to correspond reasonably well to the experimental profiles. Moreover, other than in the case of the Langmuir isotherm [36], in principle one set of isotherm and kinetic parameters could be used in all simulations; no fitting was necessary to accommodate for the protein concentration or the mobile phase composition (salt content).

In these experiments the determination of the characteristic charges was beset with a rather large experimental error (±1 U). It is quite possible that this was due to the fact that the experiments were carried out at ambient temperature (22 ± 2 °C). At the same time is the retention time of the breakthrough curve very sensitive to small changes in the values of the characteristic charge. Some fitting of this parameter was hence necessary to fine-tune the agreement between simulation and experiment, the exact values used in the experiments are given in the corresponding figure legends. It should be noted that the changes in the characteristic charge

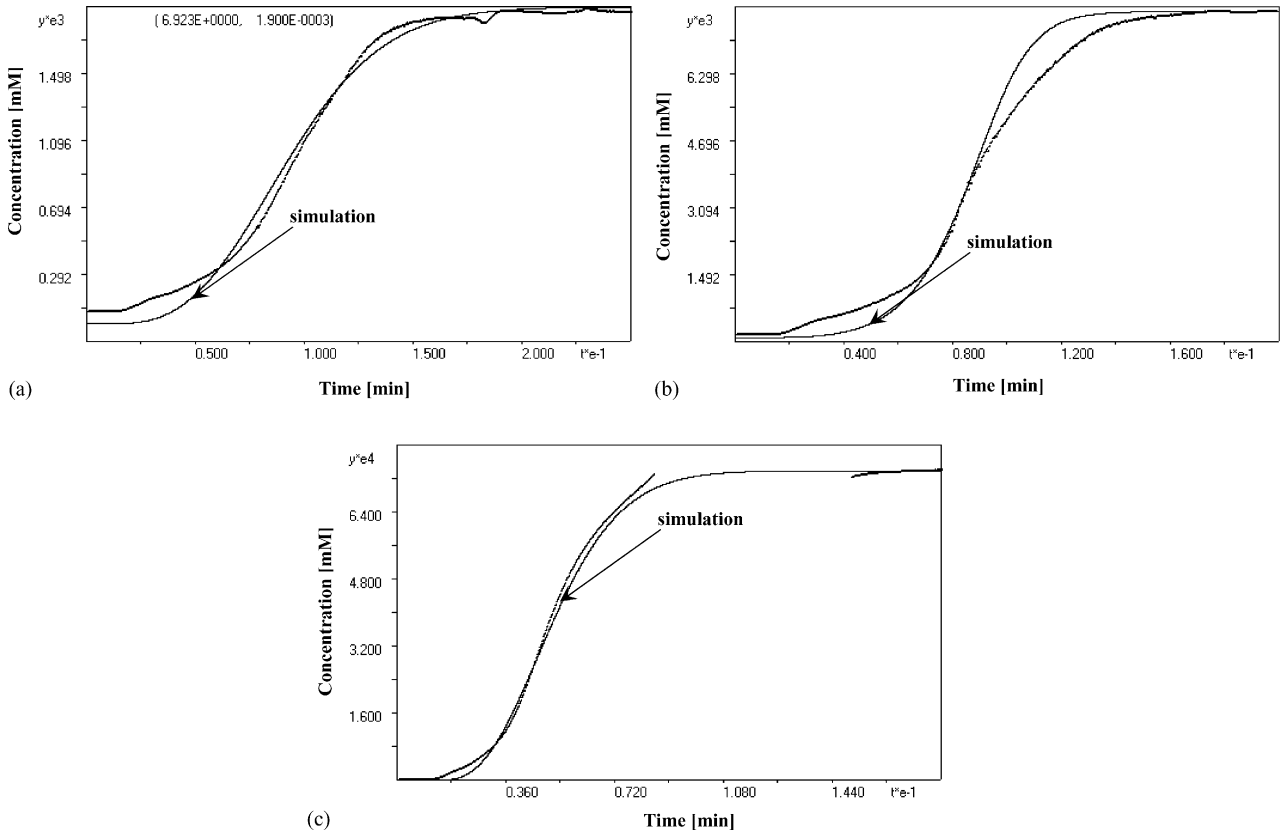

Fig. 6. Comparison between the experimental breakthrough curves and chromatograms for α-chymotrypsinogen as a function of the mobile phase composition and the protein concentration. Column: BioScale S2, flow rate 0.5 mL/min, (a) protein concentration: 0.0018 mM (0.05 mg/mL), mobile phase: 120 mM phosphate buffer pH 7.2 (characteristic charge: 0.46), (b) protein concentration: 0.0078 mM (0.2 mg/mL), mobile phase: 120 mM phosphate buffer pH 7.2 (characteristic charge: 0.46), (c) protein concentration: 0.00078 mM (0.02 mg/mL), mobile phase: 120 mM phosphate buffer pH 7.2 + 1% NaCl (characteristic charge: 0.16).

as a result of the fine-tuning are well below the experimental error.

The relevant SMA (Table 2) and transport parameters (Table 3) were then used to model the cytochrom *c* breakthrough curves on the monolithic column for different mobile phase compositions and proteins loads, Fig. 5. Again, the correspondence between the experimental and calculated breakthrough curves was good, however the value of the characteristic charge needed to be adjusted within the range of the experimental error as a function of the mobile phase composition, see legends for the exact value used in each experiment. We observed no principal difference in the behaviour of the two column types during the simulation.

In a similar fashion were the breakthrough curves of α-chymotrypsinogen simulated on both column types and good agreement was found, see Fig. 6 for examples from the particle-based column. Again some adjustment of the characteristic charge was necessary as a function of the mobile phase salt content to optimise the fit. In particular a value of 0.16 instead of 0.46 had to be used when the mobile phase (120 mM phosphate buffer, pH 7.2) contained an additional 1% of NaCl. Apart from that, no other dependency was found. It remains to be seen whether this 'change' in the characteristic charge as a function of the mobile phase composition is a physical reality or whether this is merely an artefact introduced by the model. As pointed out before, the determination of the characteristic charge is at present beset with an experimental error that prevents a detailed investigation of this question.

Most breakthrough curves and elution peaks in Figs. 4–6 show an early breakthrough step or a 'shoulder'. This is in fact the major discrepancy between the simulated and the experimental data. This step is observed not only in the case of α-chymotrypsinogen, where some impurities were present, but also for the extremely pure cytochrom *c*. It is hence most likely not due to an impurity, but rather to a presently neglected facet of the protein adsorption under experimental conditions. We are currently investigating this phenomenon for an additional number of proteins and synthetic peptides as well as other ion exchange materials. It seems likely that this step can be taken into account by using a modified isotherm algorithm.

4. Conclusions

The adsorption of proteins on charged surfaces is a complex process, as steric effects, changes in the protein structure and next neighbour effects on the surface cannot be excluded. Although often a given experimental isotherm can be fitted to the Langmuir equation, the predictive value of the then derived model parameters for the simulation of related but different experimental conditions is low. We propose that instead an algorithm should be chosen for the adsorption equilibrium that is based on an assumption concerning the physical behaviour of the involved compounds (proteins). In this paper the SMA isotherm is used successfully in combination with the POR model for the simulation of protein breakthrough curves in ion exchange chromatography.

The use of an adsorption model based on assumptions concerning the physical behaviour of the protein under chromatographic conditions improves the applicability and the predictive value of the derived simulation. In particular the protein load and the salt content of the mobile phase do not have to be taken into consideration beforehand, which is already an improvement compared to the use of the Langmuir formalism for this purpose. At present the fact that one of the SMA parameters, namely the characteristic charge, appears to depend on the mobile phase compositions remains a nuisance. Further research is needed to determine whether this dependency is routed in fact or whether this is an artefact produced by the model that can be removed by including other until now neglected aspects of protein chromatography on ion exchangers.

5. Nomenclature

a_p	external surface area of the adsorbent particles
Bi	$k_{ext}d_p/2D_{eff}$ = Biot number
C	concentration in the mobile phase
d_p	average particle diameter
D_m	molecular diffusion coefficient
$D_{m,P}$	fitted molecular diffusion coefficient for the protein inside the stationary phase (stag nant fluid)
D_{eff}	effective diffusion coefficient
D_L	axial dispersion coefficient
K	equilibrium constant
k'	capacity factor
k_{ext}	external mass transfer coefficient
k_i	overall mass transfer coefficient
k_{int}	internal mass transfer coefficient
L	column length
M	molecular weight
Pe	$uL/(DL\varepsilon_e)$ = Peclet number
Q	stationary phase concentration
r	radial coordinate
Re	$(\rho u d_p)/\eta$ = Reynolds number
R_p	equivalent particle radius
Sc	$\eta/(\rho D_m)$ = Schmidt number
Sh	$(k_{ext}d_p)/D_m$ = Sherwood number
St	$k_{ext}a_pL\varepsilon_e/u$ = Stanton number
T	absolute temperature
t	time
t_p	time during which a feed of constant concentration is introduced into the column
u	mobile phase velocity
V_{eq}	elution volume
V_0	column hold up volume
V_a	stationary phase volume
z	axial coordinate

Greek letters

β	phase ratio
ε_e	external porosity
ε_p	particle porosity
ε_t	total column porosity
γ	tortuosity factor
η	viscosity
Λ	ion capacity of the column
ν	characteristic charge
ρ	density
σ	steric factor

Subscripts

i	component index
P	protein
S	salt

Superscripts

O	inlet value
*	equilibrium value
overbar	denotes average concentration in the stagnant fluid phase

References

[1] E. Boschetti, J. Chromatogr. A 658 (1994) 207.
[2] T. Gu, G.J. Tsai, G.T. Tsao, in: A. Fiechter (Ed.), Advances in Biochemical Engineering/Biotechnology, vol. 49, Springer-Verlag, Berlin Heidelberg, 1993.
[3] D.M. Ruthven, Principles of Adsorption and Adsorption Processes, Wiley, New York, 1984.
[4] G. Guiochon, S.G. Shirazi, A.M. Katti, Fundamentals of Preparative and Nonlinear Chromatography, Academic Press, Boston, MA, 1994.
[5] W. Piatkowski, F. Gritti, K. Kaczmarski, G. Guiochon, J. Chromatogr. A 989 (2003) 207.
[6] L.E. Weaver, G. Carta, Biotechnol. Prog. 12 (1996) 342.
[7] G. Garke, R. Hartmann, N. Papamichael, W.D. Deckwer, F.B. Anspach, Sep. Sci. Technol. 34 (1999) 2521.
[8] P.M. Boyer, J.T. Hsu, Chem. Eng. Sci. 47 (1990) 241.
[9] B.A. Duri, G. McKay, J. Chem. Technol. Biotechnol. 55 (1992) 245.
[10] W.-D. Chen, Y. Sun, J. Chem. Ind. Eng. (China) 53 (2002) 88.
[11] S. Zhang, Y. Sun, AIChE J. 48 (2002) 188.
[12] B.J. Horstmann, H.A. Chase, Chem. Eng. Res. Des. 67 (1989) 243.
[13] M. Suzuki, Adsorption Engineering, Elsevier, Amsterdam, 1990.
[14] P. Sajonz, H. Guan-Sajonz, G. Zhong, G. Guiochon, Biotechnol. Prog. 12 (1997) 170.
[15] K. Miyabe, G. Guiochon, J. Chromatogr. A 866 (2000) 147.
[16] A. Seidel-Morgernstern, S.C. Jacobson, G. Guiochon, J. Chromatogr. 637 (1993) 19.
[17] K. Kaczmarski, D. Antos, H. Sajonz, P. Sajonz, G. Guiochon, J. Chromatogr. A 925 (2001) 1.
[18] M. Morbidelli, A. Servida, G. Storti, S. Carra, Ind. Eng. Chem. (Fundam.) 21 (1982) 123.
[19] M. Morbidelli, G. Storti, S. Carra, G. Niederjaufner, A. Pontoglio, Chem. Eng. Sci. 39 (1984) 383.
[20] K. Kaczmarski, D.J. Antos, J. Chromatogr. A 756 (1996) 73.
[21] E.C. Markham, A.F. Benton, J. Am. R. Chem. Soc. 53 (1931) 497.
[22] R.H. Fowler, E.A. Guggenhein, Statistical Thermodynamics, Statistical Mechanics for Students of Physics and Chemistry, Macmillan, New York, 1939.
[23] W. Fritz, E.U. Schlunder, Chem. Eng. Sci. 29 (1974) 1279.
[24] N.K. Boardman, S.M. Partridge, Biochem. J. 59 (1955) 543.
[25] W. Kopaciewicz, M.A. Rounds, J. Fausnaugh, F.E. Regnier, J. Chromatogr. 283 (1984) 37.
[26] A. Velayudhan, Cs. Horvath, J. Chromatogr. 367 (1986) 160.
[27] A. Velayudhan, Cs. Horvath, Studies in Non Linear Chromatography, Dissertation, Yale University, 1990.
[28] C.A. Brooks, S.M. Cramer, AIChE J. 38 (1992) 1962.
[29] D. Shishir Gadam, G. Jayaraman, S. Cramer, J. Chromatogr. 630 (1993) 37.
[30] A. Kundu, S. Vunnum, G. Jayaraman, S.M. Cramer, Biotechnol. Bioeng. 48 (1995) 452.
[31] Y. Li, N.G. Pinto, J. Chromatogr. A 658 (1994) 445.
[32] B. Schmidt, Ch. Wandrey, R. Freitag, J. Chromatogr. A 1018 (2003) 155.
[33] S. Vunnum, S. Gallant, S. Cramer, Biotechnol. Prog. 12 (1996) 84.
[34] S.R. Gallant, S.M. Cramer, J. Chromatogr. A 771 (1997) 9.
[35] C.A. Brooks, S.M. Cramer, J. Chromatogr. A 693 (1995) 187.
[36] M. Jozwik, Ph.D. thesis No 2960, Swiss Federal Institute of Technology Lausanne, Switzerland, 2004.
[37] J.C. Giddings, Unified Separation Science, Wiley, New York, 1991.
[38] P.A. Bristow, J.H. Knox, Chromatographia 10 (1977) 279.
[39] K. Kaczmarski, G. Storti, M. Mazzotti, M. Morbidelli, Comput. Chem. Eng. 21 (1997) 641.
[40] A.J. Berninger, R.D. Whitley, X. Zhang, N.-H.L. Wang, Comput. Chem. Eng. 15 (1991) 749.
[41] D. Gunn, Chem. Eng. Sci. 42 (1987) 363.
[42] M.E. Young, P.A. Carroad, Biotechnol. Bioeng. 22 (1980) 947.
[43] E.J. Wilson, C.J. Geankoplis, Ind. Eng. Chem. (Fundam.) 5 (1966) 9.
[44] R.B. Bird, W.E. Steward, E.N. Lightfoot, Transport Phenomena, Wiley, New York, 1994.
[45] A. Kundu, S. Vunnum, G. Jayaraman, S.M. Cramer, Biotechnol. Bioeng. 48 (1995) 452.
[46] J. Gerstner, S.M. Cramer, Biotechnol. Prog. 8 (1992) 540.